Origin of the Kink in Current-Density Versus Voltage Curves and Efficiency Enhancement of Polymer-C_{60} Heterojunction Solar Cells

Fernando Araujo de Castro, Jakob Heier, Frank Nüesch, and Roland Hany

***Abstract*—Current–voltage (*J–V*) curves of photovoltaic devices can reveal important microscopic phenomena when parameterization is properly related to physical processes. Here, we identify a pronounced effect of thermal annealing on the organic-cathode metal interface and show that this interface is related to the origin of the kink often observed in *J–V* curves close to the open circuit. We propose that isolated metal nanoclusters that form upon cathode evaporation lead to defect states close to the interface and change the electric field distribution in the device. We express this scenario with a modified equivalent circuit and consistently fit *J–V* curves as a function of the annealing process. The developed model is general in the sense that any physical process that leads to the change in electric potential as described in this paper will possibly lead to a kink in the *J–V* curves. Knowing the origin of the kink allowed us to largely increase the device efficiency of the archetypal material combination Poly[2-methoxy-5-(2-ethylhexyloxy)-1,4-phenylene-vinylene] (MEH-PPV) -C_{60}. We fabricated solar cells with an efficiency of 1.85% under 100 mW/cm^2 AM1.5 illumination by using a deliberately designed interpenetrating bilayer film morphology, aluminium as cathode and thermal annealing. This is so far the highest reported efficiency for this particular combination of materials.**

***Index Terms*—Annealing, organic-metal interface, photovoltaic cell, polymer solar cell.**

I. Introduction

DONOR–ACCEPTOR (D–A) heterojunction solar cells based on organic semiconducting small molecules and polymers are attracting much attention, in particular due to the potential of cheap photovoltaic energy production [1]–[4]. To understand its operation principles and limiting factors, critical processes in the bulk film and at the organic-electrode interfaces need to be addressed.

One of the key issues for high light-to-current conversion is the active thin-film morphology [5]–[7]. However, the principles that control the arrangement of the D–A components at the nanoscale are not well understood and systematic experimental studies that correlate varying morphologies with device performance are rare. The difficulty arises due to the large number of parameters that influence the film formation when a polymer blend is deposited from solution [8]–[11]. Post-production treatments, such as thermal or solvent annealing, can further improve the initial morphology via phase-separation and crystallization processes [12], [13]. Most of these processes have been optimized empirically so far.

A number of theoretical studies assist experiments and have modeled morphology versus performance correlations [14], [15]. Results suggest the best-performing arrangement to consist of thin layers of donor and acceptor covering the anode and cathode selectively, while in the bulk of the film the two components interpenetrate on length scales of ~5–40 nm, the typical exciton diffusion lengths of many polymers and C_{60}, respectively [16]–[18].

To experimentally mimic such an interface-enhanced bilayer film, we recently used surface-directed spinodal demixing of an active-guest polymer mixture during spin-coating to fabricate a vertically segregated bilayer film with a rough interface [19], [20]. The guest polymer was then selectively removed and the rough active polymer surface was covered with a second active component. We demonstrated the developing morphology for different solvents, compositions, and guest molecular weights. The submicrometer structures were easily reproduced and could be "controlled" by adjusting the experimental parameters. With the use of polystyrene as guest polymer, MEH-PPV as electron donor and C_{60} as acceptor, this resulted in much-improved solar cell performance, with external power efficiencies ($\eta \sim 0.6\%$) more than three times higher than reported for that particular material combination so far. Here, we exploit this structuring concept further to optimize organic solar cell performance. Details of the device fabrication are summarized in Section II [19], [20].

Besides the film morphology, also the organic-electrode interfaces critically influence device performance. For instance, the insertion of a thin buffer layer between C_{60} and the cathode often improves device performance [21]–[24]. The processes related to charge generation, transfer and collection [25] are finally reflected in the quality of the current-density versus voltage (*J–V*) characteristics [15]; therefore, these curves are a valuable source of information [26], [27]. By describing the *J–V* curves with an equivalent circuit, parameterization yields, for examples, values for series (R_s) and parallel (R_p) resistances that can be related to microscopic physical processes.

Manuscript received November 4, 2009; revised January 8, 2010; accepted January 8, 2010. Date of publication February 18, 2010; date of current version December 3, 2010.

F. Araujo de Castro was with the Laboratory for Functional Polymers, Swiss Federal Laboratories for Materials Testing and Research (EMPA), CH-8600 Duebendorf, Switzerland. He is now with the National Physical Laboratory, Materials Division, Teddington, TW11 0LW, U.K. (e-mail: fernando.castro@npl.co.uk).

J. Heier, F. Nüesch, and R. Hany are with the Laboratory for Functional Polymers, Swiss Federal Laboratories for Materials Testing and Research (EMPA), CH-8600 Duebendorf, Switzerland (e-mail: jakob.heier@empa.ch; frank.nueesch@empa.ch; roland.hany@empa.ch).

Color versions of one or more of the figures in this paper are available online at http://ieeexplore.ieee.org.

Digital Object Identifier 10.1109/JSTQE.2010.2040807

In real solar cells, however, nonideality often occurs. Decreased R_p and increased R_s reflect current leakage or charge transport/extraction problems, respectively. In particular, the diode parameters in the dark and under illumination can vary strongly [27], [28]. More complex features are difficult or impossible to analyze using the traditional equivalent circuit derived for inorganic solar cells [29]. For instance, a "kink" is sometimes observed in the *J–V* curve close to $V_{\rm oc}$ that results in reduced fill factor (FF) and cell efficiency. The origin of this "s-shape" is a matter of continuing research [21], [22], [30]–[32]. One theoretical study [33] relates its appearance to a variety of possible effects, such as reduced D–A electron transfer rate, slow intermolecular charge hopping or to metal–organic interfaces with a potential barrier for charge collection. In inorganic solar cells, the s-shape is related to interfacial defects that lead to increased charge recombination [34].

In this paper, we systematically optimized solar cells using the MEH-PPV-C_{60} material combination and studied bulk morphology and organic/metal interface issues in detail. MEH-PPV was used as one of the first electron donor polymer together with fullerenes in photovoltaic devices already some 15 years ago [35], [36]. Although this system has been extensively investigated [2], [17], [36]–[42], efficiencies reported so far were disappointing and typically below $\sim$0.2%. One of the obstacles to fabricate well-performing polymer-C_{60} solar cells is believed to be the low solubility of C_{60} that prevents the formation of polymer-fullerene blend films with high fullerene content [2].

Here, we report much-improved efficiencies ($\eta > 1.8\%$ for 100 mW/cm^2 AM1.5 simulated sunlight illumination) for optimized cell fabrication. In the first part of the paper, we compare different donor-acceptor morphologies and show that the efficiency of cells with MEH-PPV-C_{60} interpenetrating bilayer films is higher than for bulk heterojunction or planar bilayer devices. Then, we investigate the effect of annealing at different temperatures and for different times and identify a pronounced effect on the fullerene–Al interface. We further investigate the fullerene–cathode interface using different metals and including a buffer layer before metal evaporation. In the second part of the paper, we develop a physical model to relate the origin of the kink to the fullerene–cathode interface. We propose that filled trap states close to the metal–organic interface change the electric field distribution inside the device and screen the electric field at the interface, leading to the observed kink. Such traps are created by the presence of isolated Al nanoclusters in the C_{60} layer that formed during cathode evaporation. Based on this reasoning, we fitted experimental *J–V* curves by introducing a modified equivalent circuit where a second diode is added in series with the solar cell diode, but with opposite current characteristics. The consistent fitting of experimental curves supports the proposed mechanism. Our physical model explains the origin of the kink in *J–V* curves and indicates the origin of device performance increase when using buffer layers between the fullerene and the electrode. In addition, it is not restricted to the investigated materials and can be applied to different organic electronic devices.

II. Experimental

C_{60} (>99.95%, SES Research) was used as received. Poly[2-methoxy-5-(2′-ethylhexyloxy)-1,4-phenylene-vinylene] (MEH-PPV, $M_n = 40\ 000$–$70\ 000$, Aldrich) was purified before use. The polymer was dissolved in THF (1 g/150 mL), extruded through a silica gel flash chromatography column, precipitated in hexane, filtrated through a membrane filter (0.45 μm) and finally dried overnight in a vacuum oven at 40 °C. Blend and bilayer photovoltaic devices were fabricated on cleaned [19] ITO-coated glass (Thin Film Devices, resistivity $< 20\,\Omega$/square). A layer of PEDOT:PSS (Aldrich, conductivity ~ 1 S/cm) was spin-coated on ITO, followed by heating for 10 min at 140 °C in air. Then, samples were transferred to a glove box under N_2 atmosphere. Unless otherwise stated, active films were deposited from chlorobenzene solutions inside the box.

Planar double layers were prepared by spin-coating a 30-nm thick MEH-PPV film from a 5 mg/mL solution. Blend films (1:2 wt/wt) of MEH-PPV and polystyrene ($M_w = 3000$) were spin-coated to fabricate nanostructured MEH-PPV layers after selective (and complete) removal of polystyerene with cyclohexane. These, on average $\sim$30 nm thick MEH-PPV films, covered PEDOT-PSS completely, but showed a distinct surface roughness with lateral and vertical length scales of $\sim$50 nm and $\sim$5–10-nm peak-to-valley, respectively [see Fig. 2(d)]. The principles of this surface-directed spinodal demixing process of a polymer mixture to create bilayer interface undulations is described in detail in [19] and [20]. For both bilayer configurations, a 40-nm thick film of C_{60} was then thermally evaporated onto MEH-PPV. For the fabrication of blended films, 5 mg/mL MEH-PPV was dissolved in either CB or diCB, and an excess of fullerene was added to form C_{60}-saturated solutions. Solutions were stirred at 60 °C for 1 h and then at room temperature overnight. The nondissolved C_{60} was removed using 0.45 μm filters. Blend films were prepared by spin coating at 3000 r/min for 60 s. Thermal annealing was carried out on a digital controlled hot plate inside the glove box either before or after cathode deposition through a shadow mask in a vacuum chamber ($\sim 10^{-6}$ mbar). The cathode was either Al, Ag, a double layer of Ca (20 nm)/Al (40 nm), or a double layer of BCP (2 nm)/Al (40 nm). The typical evaporation rate for Al was 0.1 nm/s for the first 5 nm and then 0.2 nm/s. Devices with active areas of 7.1 or 3.2 mm^2 were produced. Solar cells were characterized under inert atmosphere using a Xe lamp as light source with part of the infrared radiation reduced through a water filter. A filter set (Oriel) was used to simulate AM1.5G conditions. Details on device fabrication and characterization are described in [19]. For the fitting, numerical calculations were performed on Visual C++ by iteratively minimizing the mean least error, which is given by the sum over the differences between measured and fitted curves at each voltage. The fitting of some of the *J–V* curves was truncated before the onset of the current increase after saturation in forward bias since our model is not able to predict the current behavior in that region.

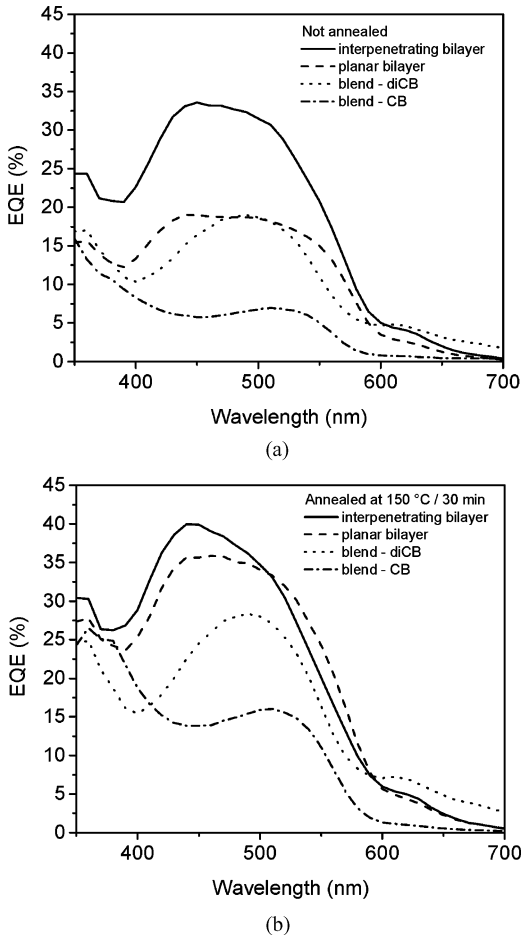

Fig. 1. External quantum efficiencies (EQE) of ITO/PEDOT-PSS/MEH-PPV/C_{60}/Al solar cells before (a) and after (b) annealing the complete devices at 150 °C for 30 min. Comparison between different active film morphologies: structured interpenetrating bilayer (full line), planar bilayer (dashed line) and bulk heterojunctions spin-coated from dichlorobenzene (diCB, dotted line) or chlorobenzene (CB, dashed-dotted line).

III. Results and Discussion

A. *Effect of Morphology*

Fig. 1 shows external quantum efficiency (EQE) spectra for planar and interpenetrating bilayer (BL) solar cells as well as bulk heterojunction (BH) devices with active layers deposited either from chlorobenzene (CB) or dichlorobenzene (diCB).

Annealing the complete cells (i.e., with top Al cathode) at 150 °C for 30 min increased the monochromatic efficiencies. The relative increase was larger in the 450–550 nm region of MEH-PPV absorption than at wavelengths below 450 nm, where predominantly C_{60} absorbs, and was more pronounced for the blend and planar bilayer heterojunction devices. These changes are due to a combination of temperature-induced effects at the organic–electrode interfaces (see in the following) and in the active bulk film morphology. For example, enhanced MEH-PPV interchain packing [43], [44] as well as crystallization of C_{60} upon annealing [45], [46] can influence the charge transport and collection efficiency, while interdiffusion of C_{60} with MEH-PPV [40] results in an increased D–A interface and improved charge generation. The different exciton diffusion lengths in MEH-PPV ($\sim$5 nm) [18] and C_{60} ($\sim$40 nm) [16] explain the larger relative EQE increase for MEH-PPV when increasing the heterojunction interface.

Fig. 2(a) shows the white light current-density versus voltage curves of the same devices after annealing. The efficiency values are depicted in Fig. 2(b). $V_{\rm oc}$ is smaller for BH cells, since it is difficult to avoid that the components interconnect partially both electrodes, leading to a loss of voltage [47]. A second mechanism influencing $V_{\rm oc}$ relates to the directional diffusion current. The photocurrent is composed of a drift and a diffusion component. In bulk heterojunctions, the direction of the donor (D)–acceptor (A) interfaces can be oriented at random with respect to the electrodes, and the net current due to diffusion of carriers is small. On the other hand, in the bilayer, the heterojunctions are aligned to direct the charges to the appropriate electrodes. This yields nonzero diffusion current at flatband conditions, and an extra field is required to reach $V_{\rm oc}$ [48], [49].

The pronounced phase separation in spin-coated BH-CB films [see Fig. 2(c)] explains the small short-circuit current for this device. The low solubility in CB probably triggers the fullerene precipitation at an early stage of the spin-coating process while the polymer is still dissolved, resulting in large domain sizes ($>$30 μm) that favor exciton relaxation after light absorption rather than charge generation after exciton diffusion to the heterointerface. This could be prevented by changing the solvent to diCB, where C_{60} is more soluble [37]. For these BH-diCB cells, no phase segregation was observed with the optical microscope, which indicates that donor and acceptor phases were in more intimate contact. This is confirmed by the much increased $J_{\rm sc}$ ($\sim$ 4.6 mA/cm^2). However, recombination losses for this film, indicated by the strong dependence of current on reverse bias (see Fig. 2(a), dotted line between $-0.2 < V < 0$) [50], are probably a signature of a nonideal internal morphology, dominated by indirect paths to the contacts and charge trapping islands of one component into the other.

The structured interpenetrating bilayer performed best. The device provided a reasonably high $J_{\rm sc}$ ($\sim$ 5 mA/cm^2) while maintaining a large $V_{\rm oc}$ ($\sim$0.62V). It also showed the highest FF ($\sim$48%), which is attributed to improved charge transport and collection. Possible reasons that account for the FF increase in the structured bilayer configuration are a decreased distance to the anode for better hole extraction [19], photodoping [51], or different charge transport properties in the polymer film when spin-coated from a blend [50]. We also note that the surface roughness of the MEH-PPV layer determines the roughness of the C_{60} layer, and consequently of the fullerene–Al interface. We modeled the electric field distribution across the device in the presence of a rough electrode [19]. The electric field close to hills of the electrode is enhanced by a factor of about two at a distance of 5 nm from the metal what improves charge collection.

It has been reported that the lowest unoccupied molecular orbital (LUMO) of C_{60} aligns with the Fermi level of the metal electrode [52]. This suggests that electron injection from fullerene into Al would not be a device-limiting factor. Although this may be valid for ideal planar electrode interfaces, our results

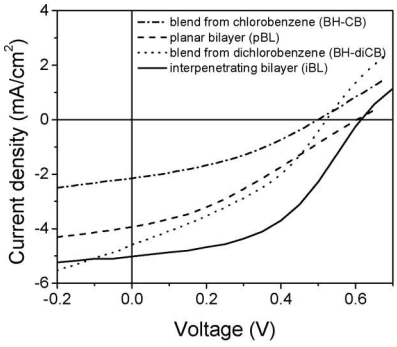

(a)

	J_{sc} (mA/cm²)	V_{oc} (V)	FF (%)	η (%)
BH-CB	2.16	0.50	36.2	0.39
pBL	3.94	0.60	32.0	0.76
BH-diCB	4.59	0.52	36.6	0.91
iBL	5.01	0.62	47.8	1.48

(b)

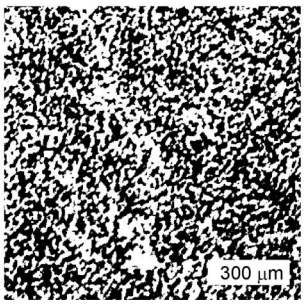

(c)

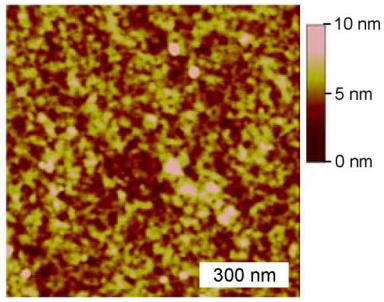

(d)

Fig. 2. (a) Current-density versus voltage curves of MEH-PPV/C_{60} devices illuminated at 100 mW/cm^2 AM1.5 simulated sunlight (95.6 mW/cm^2 for BH-diCB) after annealing the complete cells at 150 °C for 30 min. Comparison of cells with different active film morphologies: structured interpenetrating bilayer (iBL, full line), planar bilayer (pBL, dashed line) and bulk heterojunctions spin coated from dichlorobenzene (BH-diCB, dotted line) or chlorobenzene (BH-CB, dashed-dotted line). (b) Efficiency values for the devices of Fig. 2(a). $J_{\rm sc}$ is the short-circuit current density, $V_{\rm oc}$ is the open-circuit voltage, FF is the fill factor, and η is the power conversion efficiency. (c) Optical microscope picture of an MEH-PPV:C_{60} blend film spin-coated from chlorobenzene. Scale bar is 300 μm. (d) Atomic force microscopy height image of a structured MEH-PPV film as used for the iBL device.

below show that the electrode morphology is indeed decisive for the overall solar cell efficiency.

B. Effect of Thermal Annealing

To investigate the effect of elevated temperature treatment on device performance in detail, annealing experiments were carried out with solar cells fabricated in the best-performing interpenetrating bilayer geometry. Fig. 3 shows white light *J–V* curves obtained from annealed solar cells after [see Fig. 3(a)] and before [see Fig. 3(b)] Al deposition. It is apparent that cells treated without the top contact degraded at higher temperatures. In analogy to related devices, we attribute these changes to overgrowth of C_{60} crystallites with associated crevices in the film and degradation of the morphology, leading to pinholes or reduced contact area with the evaporated metal [53]. On the other hand, the performance of solar cells annealed after the deposition of the metal cathode increased for higher temperatures.

Fig. 3(c) and (d) quantifies the dependence of cell performance on annealing temperature and time. Both $V_{\rm oc}$ and FF increased with time and temperature up to around 150 °C/15 min and then saturated at ∼615 mV and 49%, respectively. $J_{\rm sc}$ did not change for annealing at 120 °C, started to increase at 150 °C and reached a maximum of ∼ 5.9 mA/cm^2 for a temperature of 200 °C. The overall power conversion efficiency increased to $\eta = 1.85\%$ for annealing at 180 °C for 30 min, then was approximately constant until 200 °C/5 min. For even higher temperature and longer times, devices rapidly started to degrade (data not shown).

C. C_{60}-Cathode Interface

As apparent from Fig. 3(a), the performance increase with annealing is concomitant with the removal of the "kink" close to $V_{\rm oc}$. However, the s-shape did not disappear when annealing was performed before electrode evaporation [see Fig. 3(b)]. These observations suggest that the s-shape comes from the organic–Al interface. Therefore, we fabricated a set of identical devices but using different cathode materials. This allows discriminating between temperature-induced changes of the film morphology and organic–electrode interface issues, since it is reasonable to assume that the morphology develops independently of the type of confining metal cap [53].

For silver (work function $W_f \sim 4.7$ eV) and calcium ($W_f \sim 2.9$ eV) no kink was observed, even without annealing [see Fig. 4(a)], and pristine Ca-cells showed a high FF of 51.5% and $\eta = 1.2\%$. For as-prepared cells with gold cathode ($W_f \sim 5.1$ eV), a slight s-shape was observed; however, the behavior with annealing was different from Al. As shown earlier, the performance of Al-devices ($W_f \sim 4.1$ eV) increased with annealing, whereas the *J–V* curves of both Au- and Ag-cells remained almost constant [see Fig. 4(b)]. Finally, solar cells with Ca electrode degraded at higher temperature, showing a strong

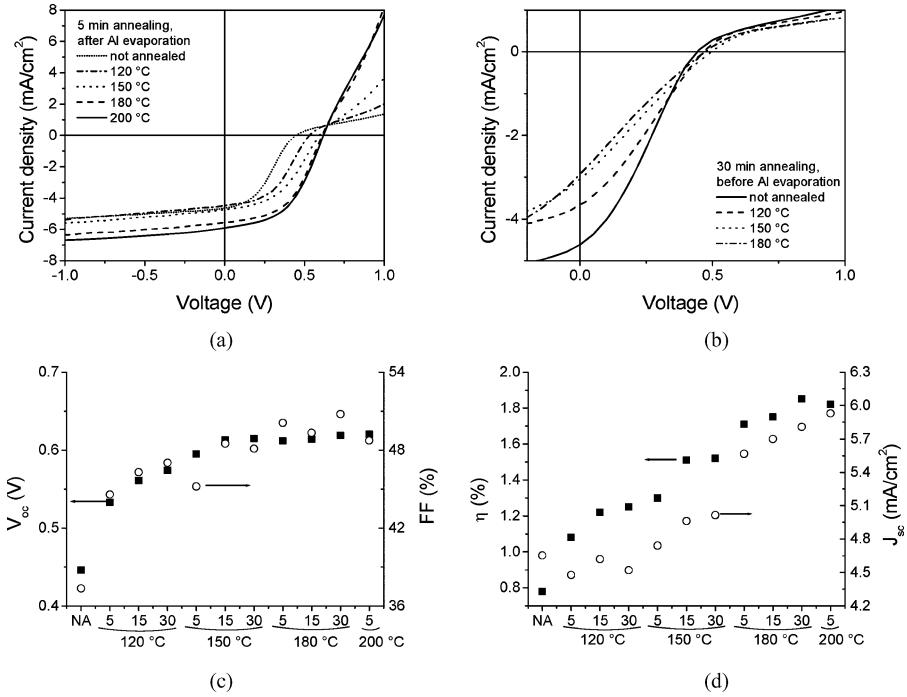

Fig. 3. Current-density versus voltage curves of interpenetrating MEH-PPV/C_{60} cells as a function of annealing temperature for 100 mW/cm^2 simulated AM1.5 sunlight conditions: (a) cells annealed after Al deposition and (b) cells annealed before Al deposition. (c) Open-circuit voltage ($V_{\rm oc}$) and fill factor (FF), (d) short-circuit current ($J_{\rm sc}$) and power conversion efficiency (η) as a function of annealing temperature and time (in minutes, after Al evaporation). NA denotes not annealed sample.

dependence of photocurrent on reverse bias, a small $J_{\rm sc}$ and a decrease in overall efficiency to $\eta = 0.49\%$.

A similar effect as with thermal annealing was achieved by using an additional buffer layer. Fig. 5 compares the *J–V* curves of two similar devices where the only difference is a 2-nm BCP layer deposited between C_{60} and Al. As evident, the s-shape was absent with BCP for the chosen deposition condition (see Section II), but a kink in the *J–V* curves also started to develop if the rate of Al evaporation was increased by a factor of approximately ten (not shown).

Our results demonstrate the particular characteristic of the Al cathode and post-production treatment for the electronic transfer processes at the organic–metal interface. The essential feature when using Al is a concave *J–V* response for as-prepared solar cells that can be almost completely removed with post-production annealing. Likewise, high FFs are obtained for practical metal evaporation rates without annealing when a buffer layer is inserted between the organic film and Al. Still then, a very high rate of Al evaporation leads to the inflection point in the *J–V* curve. This corroborates with literature demonstrating that the s-shape feature depends on the rate of evaporation, and that FF are higher for slow Al deposition [32], [54]. It also agrees with the fact that it is often necessary to include a buffer layer between C_{60} and the cathode in order to achieve high-efficiency devices [21]–[24].

D. Origin of the Kink in J–V Curves

To reveal the origin of this phenomenon, we consider a simplified morphological picture of nanometer-sized Al islands that are formed inside the organic layer during cathode evaporation (see Scheme 1). Experiments by Song *et al.* support this scenario [55]. They observed an s-shape curve when they purposely coevaporated a mixture of 1.2 wt% Al with C_{60} between a C_{60} layer and a BCP/Al electrode, while a good *J–V* curve was obtained without this mixed layer. It is well known that metals can diffuse into organic films [55]–[61]. During evaporation, metal atoms that reach the substrate surface are adsorbed and can diffuse on the surface or into the bulk, until the cohesive energy of the metal cluster or the reaction with the substrate material prevents its desorption and further diffusion [62]. For instance, metal atom diffusion into the C_{60} lattice has been observed when evaporating Au [56], Ag [57], [63] or Al [64] on fullerene films. Since C_{60} is a strong electron acceptor, these metals can transfer charge to the fullerene [24], [64], inducing electronic bandgap states with energy levels that depend on the degree of electron transfer [65] and the size of the metal clusters [63], [66], [67]. For Ag clusters in C_{60}, it has been observed that there is a critical cluster size below which only weak van der Waals interactions exist between the metal and the fullerene, while for larger clusters, charge transfer occurs [63]. Upon thermal annealing, one expects a higher mobility of the metal atoms, that is facilitated by the reorganization of the C_{60} film toward a more crystalline structure [45], [68]. The diffusion is spatially isotropic for a single metal atom inside an "infinite" fullerene film [60] and can even allow atoms from the metal film to penetrate the organic layer, as in the case of Au on diindenoperylene thin films [58]. However, due to the large cohesive energy of metals and the strongly decreased diffusion constant of clusters [69], we argue that, at elevated temperatures, these clusters capture the

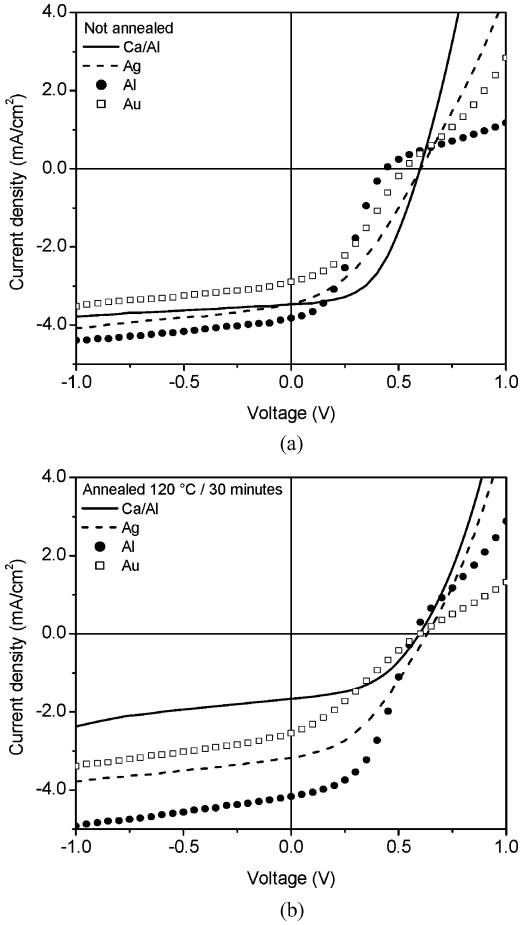

Fig. 4. *J–V* curves from interpenetrating bilayer MEH-PPV-C_{60} solar cells using different metals as cathodes: Ca–Al bilayer (full line), Ag (dashed line), Al (full circles) and Au (open squares). Before (a) and after (b) annealing the complete cell at 120 °C for 30 min.

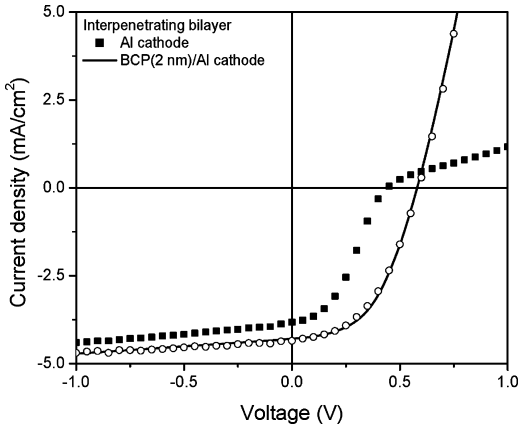

Fig. 5. Comparison of *J–V* curves for interpenetrating bilayer devices with Al (full squares) and BCP (2 nm)/Al (open circles) as cathode. Light intensity was 84 mW/cm^2. The solid line represents the fitted curve.

diffusing atoms, leading to the coalescence of the metallic islands and eventually to the merging with the bulk cathode. The effect of thermal annealing would then be to decrease the density of induced bandgap states (traps, see Scheme 1) close to the organic–cathode interface. It is clear that the extent of metal diffusion, cluster formation or coalescence strongly depends on

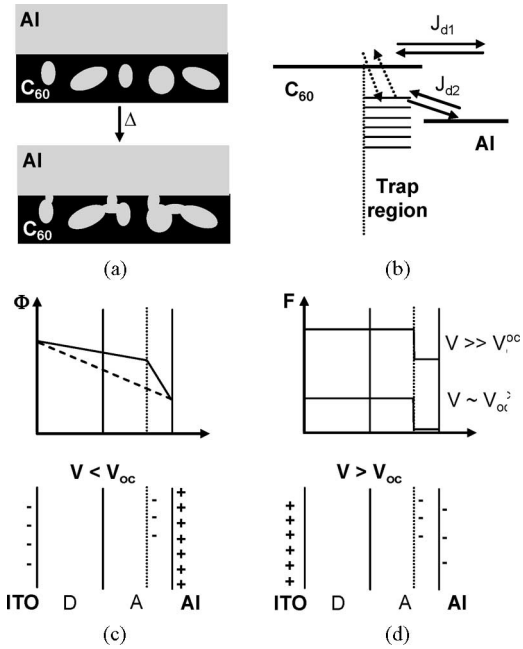

Scheme 1. (Top) (a) Proposed morphology of the Al–C_{60} interface before and after (Δ) annealing the complete solar cell, and implication (b)–(d) on the *J–V* characteristics. (b) Energy diagram with the LUMO level of C_{60}, the Fermi level of Al and the trap states in the bandgap of C_{60} introduced by the metal nanoclusters. J_{d1} represents current that flows between the C_{60} LUMO and Al directly, and J_{d2} represents the current from electrons that were trapped and detrapped. The trap region in (b)–(d) is represented by a vertical dotted line, while the donor–acceptor (D–A) heterojunction is represented by a vertical solid line. Sizes are out of scale to allow visualization. (c) Electric potential (Φ) drop inside the device with (full line) and without trapped charges (dashed line) at short circuit. (d) Absolute value of the electric field (F) as a function of the position inside the device, showing the screening effect due to trapped charges. (Bottom) distribution of the charge density including the trapped electrons inside C_{60}, for $V < V_{oc}$ (c) and $V > V_{oc}$ (d).

substrate temperature, free volume, deposition rate and metal–polymer interaction strength [57]–[59]. Therefore, details of the interface morphology are expected to depend on the metal.

We propose the following relevant electronic processes due to the presence of localized trap states in C_{60} close to the interface with Al (see Scheme 1). Under light irradiation, photogenerated electrons will populate the trap states. In steady state, this extra negative charge density changes the electric potential drop across the device. At short-circuit and for small reverse bias conditions, the potential drop in the organic layer will be reduced, while it is increased in the trap region close to the bulk metal film [see Scheme 1(c)]. The smaller electric field at the D–A heterojunction might result in increased geminate recombination of coulombically bound electron-hole pairs [50], and, consequently, reduced photocurrent. On the other hand, the influence of the trapped charges on the overall charge collection efficiency is probably small, since it is usually assumed that holes and electrons that escape the junction are collected loss-free in the bilayer D–A film configuration [4]. For increasing negative bias, the probability for detrapping/tunneling rises and we expect an increasing current J_{d2} to flow through the trap region towards the Al bulk film.

Under forward bias, the following regimes have to be distinguished [see Scheme 1(d)]. In the low field region ($V_{oc} >$

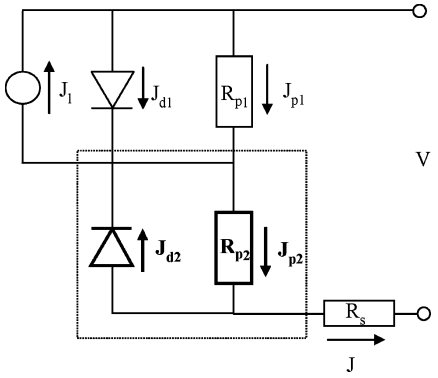

Fig. 6. Proposed equivalent circuit including a rectifying element (diode 2) with opposite current characteristics to that of the solar cell diode (diode 1). When no current J_{d2} flows through the counter diode, the circuit is reduced to the traditional equivalent circuit used to parameterize inorganic p-n junction solar cells [29], with the series resistance given by $R_s + R_{p2}$.

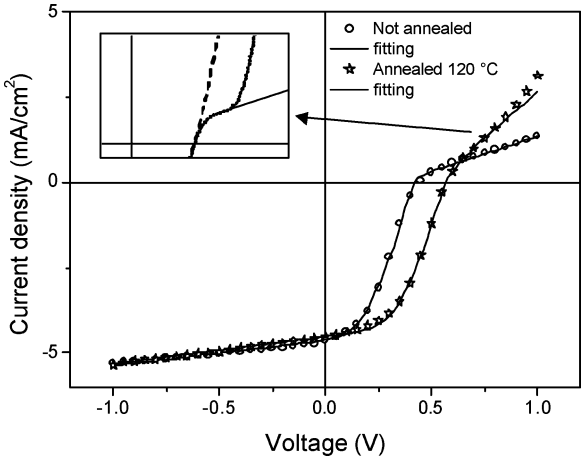

Fig. 7. Experimental and fitted (solid lines) *J–V* curves using the modified equivalent circuit of Fig. 6 for interpenetrating MEH-PPV-C_{60} bilayer solar cells with Al as cathode before annealing (circles) and after annealing the complete cell at 120 °C for 30 min (stars). The model is not able to predict the current increase after the kink, since this represents a breakdown of the second diode that was not included in the calculation. The inset exemplifies this effect showing a typical diode curve (dashed line), a schematic experimental curve with a kink (dotted line), and a simulated curve using the modified circuit (solid line).

$V > 0$), the change in electric field at the D–A heterojunction leads to a decrease of the photocurrent. The observed decrease in $V_{\rm oc}$ is explained by the presence of a negative charge density close to the contact, which leads to a voltage drop [see Scheme 1(c)]. For low positive voltages ($\sim V_{\rm oc}$), the trapped electrons efficiently screen the electric field at the C_{60}–Al interface. In this case, charge transfer across the trap region between Al and C_{60} is not favorable, and a saturation trend rather than diode current behavior is expected (onset of the kink). Since the current through the trap region (J_{d2}) is constantly very small in this low forward bias region and strongly increases in reverse bias, its behavior is similar to a rectifying component with opposite current characteristics to that of the solar cell diode.

At high forward bias ($V > V_{\rm oc}$), the trapped charges no longer screen the applied electric field effectively, and the typical exponential increase in diode forward current is re-established. The transition voltage directly depends on the trap density. When expressing the trap region as a diode, the transition voltage represents the diode breakdown. For dark measurements, the trap states will be populated under forward bias by electrons injected from Al. The effect of the filled traps is to reduce the forward current and to increase the diode onset voltage. This agrees with our observations (not shown).

Overall, the effect of nanosized Al clusters distributed at the organic–metal interface of the solar cell can descriptively be translated into an equivalent circuit with an additional rectifying diode with a current characteristic that opposes the normal cell diode. To examine this assumption, we used the equivalent circuit shown in Fig. 6 to fit experimental *J–V* curves, where the second diode represents the effect of traps at the interface. It is a generalization of the traditional equivalent circuit developed for p-n junction inorganic solar cells [29] and often used to parameterize organic photovoltaics [27]. If no current crosses the second diode ($J_{d2} = 0$), it is reduced to the traditional circuit, with the series resistance equals to $R_s + R_{p2}$. For the proposed circuit, the current versus voltage characteristics is described by

$$(\mathrm{AR}_{p1} + \mathrm{AR}_{p2})\, J = (V - \mathrm{AR}_s J) + \mathrm{AR}_{p1} J_{d1} - \mathrm{AR}_{p2} J_{d2} - \mathrm{AR}_{p1} J_l \quad (1)$$

where

$$J_{d1} = J_{s1}\{\exp[a_1(V - \mathrm{AR}_s J - \mathrm{AR}_{p2} J - \mathrm{AR}_{p2} J_{d2})] - 1\} \quad (2)$$

$$J_{d2} = J_{s2}\{\exp[-a_2(V - \mathrm{AR}_s J - \mathrm{AR}_{p1} J + \mathrm{AR}_{p1} J_{d1} - \mathrm{AR}_{p1} J_1)] - 1\} \quad (3)$$

and $a_i = q/n_i k_{\rm B} T$ (i = 1,2), with q the elementary charge, $k_{\rm B}$ the Boltzmann constant, A the area, T the absolute temperature and n the ideality factor of the respective diode.

To limit the computational time and to increase the convergence of the numerical calculation, we approximated the voltage drop across each diode by introducing the effective resistances R_{s1} and R_{s2}, such that

$$J_{d1} \approx J_{s1}\{\exp[a_1(V - \mathrm{AR}_{s1} J)] - 1\} \quad (4)$$

$$J_{d2} \approx J_{s2}\{\exp[a_2(V - \mathrm{AR}_{s2} J - \mathrm{AR}_{p1} J_1)] - 1\}. \quad (5)$$

Note that, due to the different directions of current flow in each diode, the sign of the voltage drop across diode 2 is negative but it is positive for diode 1. Therefore, a larger R_{s1} decreases the current flow through diode 1, but an increase of R_{s2} or $R_{p1} \times J_l$ effectively increases the current through diode 2. It is interesting that the current through the second diode contains a light dependent term (J_l). This qualitatively agrees with the view that traps are filled by photogenerated electrons.

Figs. 5 and 7 show that the simulated curves agree well with the experimental data. Our circuit is not able to simulate the region of exponential current increase after saturation of the forward current (see Fig. 7). As discussed before, this transition point represents the breakdown of the second diode, which was not included in the equivalent circuit model. The situation is exemplified in the inset of Fig. 7, where we exaggerated the

transition region in a schematic *J–V* curve (dotted line) and included curves representing the simulation with the modified equivalent circuit (full line) and a typical diode curve without s-shape (dashed line). Therefore, our fittings are only relevant before the onset of current increase after saturation in forward bias. Curves with no concave *J–V* response could equally well be simulated by zeroing the current through diode 2 (see Fig. 5), because the traditional circuit just represents a limiting case from the more general equivalent circuit (see Fig. 6).

Upon annealing, AR_{s2} strongly decreases from 1300 to 235 $\Omega{\cdot}cm^2$ and AR_{p2} drops from 100 $\Omega{\cdot}cm^2$ to almost zero (0.002), indicating that the current through diode 2 strongly decreases. At the same time, the parameters from diode 1 ($AR_{p1} \sim 1300$ $\Omega{\cdot}cm^2$, $AR_{s1} \sim 40$ $\Omega{\cdot}cm^2$ and ideality factor $\sim$1.89) change only slightly. This indicates that the main effect of annealing occurs at the C_{60}/Al interface, represented in the model by the second diode. These trends qualitatively agree with the microscopic picture of trap states induced by metal nanoclusters. Upon annealing the complete cell, such clusters coalesce and/or contact the metal bulk film [see Scheme 1(a)], decreasing the number of traps and the charge density close to the contact. This reduces the voltage loss and increases the cell performance (see Fig. 3).

It is interesting to examine the effects of other conceivable interface processes and their influence on the organic–metal charge transfer. One such possibility relates to the formation of complexes through chemical bonding that might improve interface charge transfer [44]. For low-temperature device fabrication conditions [70], the carbons of PCBM (a soluble C_{60} derivative) were found to be unaffected when evaporating Al. On the other hand, there are reports that covalent C_{60}–Al bonds are formed at high temperatures [71], accompanied by an increase of the Al work function. We do not speculate on the detailed mechanism of such charge transfer improvement or whether chemical reactions occur at all for our initial device fabrication conditions, but we argue that the relatively low annealing temperatures probably would not induce additional reactions. In any case, an increase of the work function for chemically bound Al should rather result in a decrease of device performance, since the electric built-in field would decrease.

It has been suggested that annealing increases the organic–metal contact area [72]. This is a likely event in our case as well, however, it probably does not determine the *J–V* characteristics. This is because an incomplete coverage of C_{60} with Al corresponds, as a first approximation, to a smaller active device area, which results in decreased photocurrent but does not change the overall *J–V* curve.

We also consider the influence of a potential energy barrier at the interface, which would most likely consist of a thin Al oxide layer in our devices that forms during cathode evaporation [73]. Depending on the position of the relative energy levels and the layer thickness, such an insulation layer could indeed act as a nonlinear series resistance and lead to concave *J–V* response following similar arguments as for our proposed trap model. However, we exclude Al_2O_3 as a possibility to explain the changes in *J–V* characteristics, since this oxide would be inert in our temperature range of annealing. A second argument relates to the experiments using a BCP buffer layer (see Fig. 5). These solar cells did not show a kink in the *J–V* curves, although then Al was used as cathode and evaporated under the same conditions.

Kinks have also been reported for material combination other than C_{60} and Al and also for solar cells fabricated in an inverted geometry, where the organic material was deposited onto the metal [32], [44], [54]. If similar processes explain the concave *J–V* curves remains open at this point. However, we argue that our model is rather general since it anticipates that any process that leads to the screening of the electric field close to the contact, with the importance of such screening effect being voltage dependent, will affect the onset of current increase in *J–V* curves. Finally, some authors have speculated that a nonspecific "slow charge transfer" at the contact induces a concave *J–V* curve. Indeed, our model implies retarded charge transfer and explains its origin.

IV. Conclusion

In conclusion, MEH-PPV-C_{60} solar cells with power-conversion efficiency approaching 2% were demonstrated by applying a two-step process to fabricate an interface-enhanced bilayer D–A film, using Al as cathode and post-production thermal annealing. One aspect for possible further improvement relates to the polymer purity. Although not studied in detail, the purification process of MEH-PPV was fundamental, and efficiencies of solar cells fabricated with as-received polymer never exceeded $\sim$0.2% and strongly varied from batch-to-batch. Therefore, a performance increase might be expected from improved chemical synthesis of MEH-PPV, to minimize constitutional defects and to control molar mass and distribution [74]. In addition, the bilayer film architecture is not yet optimized. Typical aspect ratios of topographical features were far below 1 (height $\sim$5–10 nm, widths $\sim$50 nm), which limits the heterojunction interface area and does not allow using thicker active films. The amplitude of features is limited by the interfacial tension between the active and the guest polymer. Therefore, other guests for the initial spin coating process or external forces might be used to amplify the initial interface ripples [75].

Our investigation emphasized the effect of thermal annealing on the fullerene–Al interface. For as-prepared cells, a typical kink ("s-shape") occurred in the current-density versus voltage characteristics close to V_{oc}, but the concave *J–V* response was almost completely removed upon annealing. We suggest that isolated Al nanoclusters are formed upon cathode evaporation leading to defects close to the interface. Under cell operation, these trap states are filled with electrons, what modifies the electric potential drop in the device and screens the electric field at the cathode side for low forward bias. At elevated temperature, the metal islands probably coalesce and eventually merge with the bulk cathode, decreasing the trap density. We expressed this scenario with a modified equivalent circuit for a solar cell and were able to fit the experimental data. The trend of the fit parameters as a function of annealing temperature indicated a strong change at the interface and a less pronounced effect on the bulk, what correlates with our experimental observations. By

decreasing the current through the additional diode, the behavior of an ideal solar cell is re-established. Our results indicate that the main effect of a buffer layer, such as BCP, is to protect the fullerene from metal diffusion and that exciton diffusion to the cathode is not a limiting process in these cells [21].

ACKNOWLEDGMENT

The authors would like to thank R. Hauert, H. Benmansour, M. Brinkmann and A. Kupferschmid for their helpful discussions and K. Kovač for her help with the programming.

REFERENCES

[1] C. W. Tang, "Two layer organic photovoltaic cell," *Appl. Phys. Lett.*, vol. 48, pp. 183–185, 1986.

[2] G. Yu, J. Gao, J. C. Hummelen, F. Wudl, and A. J. Heeger, "Polymer Photovoltaic cells: Enhanced efficiencies via a network of internal donor-aceptor heterojunctions," *Science*, vol. 270, pp. 1789–1751, 1995.

[3] S. E. Shaheen, C. J. Brabec, N. S. Sariciftci, F. Padinger, T. Fromherz, and J. C. Hummelen, "2.5% efficiency organic plastic solar cells," *Appl. Phys. Lett.*, vol. 78, pp. 841–843, 2001.

[4] K. M. Coakley and M. D. McGehee, "Conjugated polymer photovoltaic cells," *Chem. Mater.*, vol. 16, pp. 4533–4542, 2004.

[5] H. J. Snaith and R. H. Friend, "Morphological dependence of charge generation and transport in blended polyfluorene photovoltaic devices," *Thin Solid Films*, vol. 451–452, pp. 567–571, 2004.

[6] H. Hoppe and N. S. Sariciftci, "Morphology of polymer/fullerene bulk heterojunction solar cells," *J. Mater. Chem.*, vol. 16, pp. 45–61, 2006.

[7] S. C. Veenstra, J. Loos, and J. M. Kroon, "Nanoscale structure of solar cells based on pure conjugated polymer blends," *Prog. Photovoltaics: Res. Appl.*, vol. 15, pp. 727–740, 2007.

[8] S. Walheim, M. Böltau, J. Mlynek, G. Krausch, and U. Steiner, "Structure formation via polymer demixing in spin-cast films," *Macromolecules*, vol. 30, pp. 4995–5003, 1997.

[9] M. Geoghegan and G. Krausch, "Wetting at polymer surfaces and interfaces," *Prog. Polym. Sci.*, vol. 28, pp. 261–302, 2003.

[10] P.G. De Gennes, "Dynamics of fluctuations and spinodal decomposition in polymer blends," *J. Chem. Phys.*, vol. 72, pp. 4756–4763, 1980.

[11] A. Budkowsky, "Interfacial phenomena in thin polymer films: Phase coexistence and segregation," *Adv. Polym. Sci.*, vol. 148, pp. 1–111, 1999.

[12] L. H. Nguyen, H. Hoppe, T. Erb, S. Günes, G. Gobsch, and N. S. Sariciftci, "Effects of annealing on the nanomorphology and performance of poly(alkylthiophene):fullerene bulk-heterojunction solar cells," *Adv. Funct. Mater.*, vol. 17, pp. 1071–1078, 2007.

[13] M. M. Mandoc, W. Veurman, J. Sweelssen, M. M. Koetse, and P. M. Blom, "Origin of the efficiency improvement in all-polymer solar cells upon annealing," *Appl. Phys. Lett.*, vol. 91, pp. 073518-1–073518-3, 2007.

[14] P. K. Watkins, A. B. Walker, and G. L. B. Verschoor, "Dynamical Monte Carlo modelling of organic solar cells: The dependence of internal quantum efficiency on morphology," *Nano Lett*, vol. 5, pp. 1814–1818, 2005.

[15] R. A. Marsh, C. Groves, and N. C. Greenham, "A microscopic model for the behavior of nanostructured organic photovoltaic devices," *J. Appl. Phys.*, vol. 101, pp. 083509-1–083509-7, 2007.

[16] P. Peumans, A. Yakimov, and S. R. Forrest, "Small molecular weight organic thin-film photodetectors and solar cells," *J. Appl. Phys.*, vol. 93, pp. 3693–3723, 2003.

[17] J. J. M. Halls, K. Pichler, R. H. Friend, S. C. Moratti, and A. B. Holmes, "Exciton diffusion and dissociation in a poly(p-phenylenevinylene)/C_{60} heterojunction photovoltaic cell," *Appl. Phys. Lett*, vol. 68, pp. 3120–3122, 1996.

[18] D. E. Markov, E. Amsterdam, P. W. M. Blom, A. B. Sieval, and J. C. Hummelen, "Accurate measurement of the exciton diffusion length in a conjugated polymer using a heterostructure with a side-chain cross-linked fullerene layer," *J. Phys. Chem. A*, vol. 109, pp. 5266–5274, 2005.

[19] F. A. Castro, H. Benmansour, C. F. O. Graeff, F. Nüesch, E. Tutis, and R. Hany, "Nanostructured organic layers via polymer demixing for interface-enhanced photovoltaic cells," *Chem. Mater.*, vol. 18, pp. 5504–5509, 2006.

[20] F. A. Castro, C. F. O. Graeff, J. Heier, and R. Hany, "Interface morphology snapshopts of vertically segregated thin films of semiconducting polymer/polysterene blends," *Polymer*, vol. 48, pp. 2380–2386, 2007.

[21] M. Vogel, S. Doka, Ch. Breyer, M. Ch. Lux-Steiner, and K. Fostiropoulos, "On the function of a bathocuproine buffer layer in organic photovoltaic cells," *Appl. Phys. Lett.*, vol. 89, pp. 163501-1–163501-3, 2006.

[22] Y. Berredjem, N. Karst, A. Boulmokh, A. Drici, and J. C. Bernède, "Optimisation of the interface "organic material/aluminium" of CuPc/C_{60} based photovoltaic cells," *Eur. Phys. J. Appl. Phys.*, vol. 40, pp. 163–167, 2007.

[23] H. Gommans, B. Verreet, B. P. Rand, R. Muller, J. Poortmans, P. Heremans, and J. Genoe, "On the role of bathocuproine in organic photovoltaic cells," *Adv. Funct. Mater.*, vol. 18, pp. 3686–3691, 2008.

[24] Q. L. Song, C. M. Li, M. L. Wang, X. Y. Sun, and X. Y. Hou, "Role of buffer in organic solar cell using C_{60} as an acceptor," *Appl. Phys. Lett.*, vol. 90, pp. 071109-1–071109-3, 2007.

[25] C. R. McNeill, S. Westenhoff, C. Groves, R. H. Friend, and N. C. Greenham, "Influenece of nanoscale phase separation on the charge generation dynamics and photovoltaic performance of conjugated polymer blends: Balancing charge generation and separation," *J. Phys. Chem. C*, vol. 111, pp. 19153–19160, 2007.

[26] W. U. Huynh, J. J. Dittmer, N. Teclemariam, D. J. Milliron, A. P. Alivisatos, and K. W. J. Barnham, "Charge transport in hybrid nanorod-polymer composite photovoltaic cells," *Phys. Rev. B*, vol. 27, p. 115326, 2003.

[27] S. Yoo, B. Domercq, and B. Kippelen, "Intensity-dependent equivalent circuit parameters of organic solar cells based on pentacene and C_{60}," *J. Appl. Phys.*, vol. 97, pp. 103706-1–103706-9, 2005.

[28] B. A. Gregg and M. C. Hanna, "Comparing organic to inorganic photovoltaic cells: Theory, experiment and simulation," *J. Appl. Phys.*, vol. 93, pp. 3605–3614, 2003.

[29] S. M. Sze, *Physics of Semiconductor Devices,* 2nd ed. Singapore: Wiley, 1981, ch. 14.

[30] I. Mora-Seró and J. Bisquert, "Effect of reduced selectivity of contacts on the current-potential characteristics and conversion performance of solar cells," *Solar Energy Mater. Solar Cells*, vol. 85, pp. 51–62, 2005.

[31] M. O. Reese, M. S. White, G. Rumbles, D. S. Ginley, and S. E. Shaheen, "Optimal negative electrodes for poly(3-hexylthiophene):[6,6]-phenyl C61-butyric acid methyl ester bulk heterojunction photovoltaic devices," *Appl. Phys. Lett.*, vol. 92, pp. 053307-1–053307-3, 2008.

[32] D. Gupta, M. Bag, and K. S. Narayan, "Correlating reduced fill factor in polymer solar cells to contact effects," *Appl. Phys. Lett.*, vol. 92, pp. 093301-1–093301-3, 2008.

[33] J. Nelson, J. Kirkpatrick, and P. Ravirajan, "Factors limiting the efficiency of molecular photovoltaic devices," *Phys. Rev. B*, vol. 69, pp. 035337-1–035337-11, 2004.

[34] A. Froitzheim, K. Brendel, L. Elstner, W. Fuhs, K. Kliefoth, and M. Schmidt, "Interface recombination in heterojunctions of amorphous and crystalline silicon," *J. Non-Cryst. Solids*, vol. 299–302, pp. 663–667, 2002.

[35] N. S. Sariciftci, L. Smilowitz, A. J. Heeger, and F. Wudl, "Photoinduced electron transfer from a conducting polymer to buckminsterfullerene," *Science*, vol. 258, pp. 1474–1476, 1992.

[36] N. S. Sariciftci, D. Braun, C. Zhang, V. I. Srdanov, A. J. Heeger, G. Stucky, and F. Wudl, "Semiconducting polymer-buckministerfullerene heterojunctions: Diodes, photodiodes and photovoltaic cells," *Appl. Phys. Lett.*, vol. 62, pp. 585–587, 1993.

[37] J. Gao, F. Hide, and H. Wang, "Efficient photodetectors and photovoltaic cells from composites of fullerenes and conjugated polymers: Photoinduced electron transfer," *Synth. Met.*, vol. 84, pp. 979–980, 1997.

[38] C. J. Brabec, F. Padinger, N. S. Sariciftci, and J. C. Hummelen, "Photovoltaic properties of conjugated polymer/methanofullerene composites embedded in a polystyrene matrix," *J. Appl. Phys.*, vol. 85, pp. 6866–6872, 1999.

[39] J. Liu, Y. Shi, and Y. Yang, "Solvation-induced morphology effects on the performance of polymer-based photovoltaic devices," *Adv. Funct. Mater.*, vol. 11, pp. 420–424, 2001.

[40] M. Drees, K. Premaratne, W. Graupner, J. R. Heflin, R. M. Davis, D. Marciu, and M. Miller, "Creation of a gradient polymer-fullerene interface in photovoltaic devices by thermally controlled interdiffusion," *Appl. Phys. Lett.*, vol. 81, pp. 4607–4609, 2002.

[41] C. Yang, Y. Li, J. Hou, C. He, Z. Tan, B. Fan, Y. Zhou, Q. Sun, Y. Li, Y. Li, and D. Zhu, "Thinner-film plastic photovoltaic cells based on different C_{60} derivatives," *Polym. Adv. Technol.*, vol. 17, pp. 500–505, 2006.

[42] H. Jin, Y.-B. Hou, X.-G. Meng, and F. Teng, "Charge photogeneration and recombination in poly[2-methoxy-5-(2'-ethyl-hexoxy-p-phenylene vinylene]:fullerene composite films studied by photocurrent response," *Thin Solid Films*, vol. 516, pp. 1142–1146, 2008.

[43] P. S. Davids, I. H. Campbell, and D. L. Smith, "Device model for single carrier organic diodes," *J. Appl. Phys.*, vol. 82, pp. 6319–6325, 1997.
[44] T.-W. Lee and O. O. Park, "The effect of different heat treatments on the luminescence efficiency of polymer light-emitting diodes," *Adv. Mater.*, vol. 12, pp. 801–804, 2000.
[45] G. Chen and G. Ma, "Crystallization and orientation of C_{60} from C_{60}/polymethyl methacrylate films," *Appl. Phys. Lett.*, vol. 72, pp. 3294–3296, 1998.
[46] L. Ma, J. Ouyang, and Y. Yang, "High-speed and high-current density C_{60} diodes," *Appl. Phys. Lett.*, vol. 84, pp. 4786–4788, 2004.
[47] H. J. Snaith, N. C. Greenham, and R. H. Friend, "The origin of collected charge and open-circuit voltage in blended polyfluorene photovoltaic devices," *Adv. Mater.*, vol. 16, pp. 1640–1645, 2004.
[48] J. A. Barker, C. M. Ramsdale, and N. C. Greenham, "Modeling the current-voltage characteristics of bilayer polymer photovoltaic devices," *Phys. Rev. B*, vol. 67, pp. 075205-1–075205-9, 2003.
[49] D. Cheyns, J. Poortmans, P. Heremans, C. Deibel, S. Verlaak, B. P. Rand, and J. Genoe, "Analytical model for the open-circuit voltage and its associated resistance in organic planar heterojunction solar cells," *Phys. Rev. B*, vol. 77, pp. 165332-1–165332-10, 2008.
[50] P. W. M. Blom, V. D. Mihailetchi, L. J. A. Koster, and D. E. Markov, "Device physics of polymer:fullerene bulk heterojunction solar cells," *Adv. Mater.*, vol. 19, pp. 1551–1566, 2007.
[51] N. S. Sariciftci, "Role of buckminsterfullerene, C_{60}, in organic photoelectric devices," *Prog. Quant. Electr.*, vol. 19, pp. 131–159, 1995.
[52] T. R. Ohno, Y. Chen, S. E. Harvey, G. H. Kroll, J. H. Weaver, R. E. Haufler, and R. E. Smalley, "C_{60} bonding and energy-level alignment on metal and semiconductor surfaces," *Phys. Rev. B*, vol. 44, pp. 13747–13755, 1991.
[53] P. Peumans, S. Uchida, and S. R. Forrest, "Efficient bulk heterojunction photovoltaic cells using small-molecular-weight organic thin films," *Nature*, vol. 425, pp. 158–162, 2003.
[54] M. Glatthaar, M. Riede, N. Keegan, K. Sylvester-Hvid, B. Zimmermann, M. Nigemann, A. Hinsch, and A. Gombert, "Efficiency limiting factors of organic bulk heterojunction solar cells identified by electrical impedance spectroscopy," *Solar Energy Mater. Solar Cells*, vol. 91, pp. 390–393, 2007.
[55] Q. L. Song, F. Y. Li, H. Yang, H. R. Wu, X. Z. Wang, W. Zhou, J. M. Zhao, X. M. Ding, C. H. Huang, and X. Y. Hou, "Small-molecule organic solar cells with improved stability," *Chem. Phys. Lett.*, vol. 416, pp. 42–46, 2005.
[56] Z. Y. Rong and L. Rokhinson, "STM study of gold-overlayer formation on C_{60} monolayers," *Phys. Rev. B*, vol. 49, pp. 7749–7753, 1994.
[57] D. Sarkar and N. J. Halas, "Diffusion of silver in C_{60} thin films," *Appl. Phys. Lett.*, vol. 63, pp. 2438–2440, 1993.
[58] A. C. Dürr, F. Schreiber, M. Kelsch, H. D. Carstanjen, and H. Dosch, "Morphology and thermal stability of metal contacts on crystalline organic thin films," *Adv. Mater.*, vol. 14, pp. 961–963, 2002.
[59] B. D. Silverman, "Single-particle diffusion into a disordered matrix: Simulation of a metal-polymer interface," *Macromolecules*, vol. 24, pp. 2467–2474, 1991.
[60] F. Faupel, R. Willecke, and A. Thran, "Diffusion of metals in polymers," *Mater. Sci. Eng. R.*, vol. 22, pp. 1–50, 1998.
[61] W. Tang, H. Shi, G. Xu, B. S. Ong, Z. D. Popovic, J. Deng, J. Zhao, and G. Rao, "Memory effect and negative differential resistance by electrode-induced two-dimensional single-electron tunneling in molecular and organic electronic devices," *Adv. Mater.*, vol. 17, pp. 2307–2310, 2005.
[62] K. Demirkan, A. Mathew, C. Weiland, M. Reid, and R. L. Opila, "Reactivity and morphology of vapor-deposited Al/polymer interfaces for organic semiconductor devices," *J. Appl. Phys.*, vol. 103, pp. 034505-1–034505-7, 2008.
[63] H. Wang, J. G. Hou, O. Takeuchi, Y. Fujisuku, and A. Kawazu, "STM observations of Ag-induced reconstruction of C_{60} thin films," *Phys. Rev. B*, vol. 61, pp. 2199–2203, 2000.
[64] D. W. Owens, C. M. Aldao, D. M. Poirier, and J. H. Weaver, "Charge transfer, doping and interface morphologies of Al-C_{60}," *Phys. Rev. B*, vol. 51, pp. 17068–17072, 1995.
[65] A. F. Hebard, C. B. Eom, Y. Iwasa, K. B. Lyons, G. A. Thomas, D. H. Rapkine, R. M. Fleming, R. C. Haddon, J. M. Phillips, J. H. Marshall, and R. H. Eick, "Charge transfer at aluminum-C_{60} interfaces in thin-film multilayer structures," *Phys. Rev. B*, vol. 50, pp. 17740–17743, 1994.
[66] W. P. Halperin, "Quantum size effects in metal particles," *Rev. Mod. Phys.*, vol. 58, pp. 533–606, 1986.
[67] C. Q. Sun, "Size dependence of nanostructures: Impact of bond order deficiency," *Prog. Solid Stat. Chem.*, vol. 35, pp. 1–159, 2007.
[68] J. Gong, F. Zhang, Y. Li, G. Ma, and G. Chen, "Effects of annealing on the electrica conductivity of C_{60} films," *Thin Solid Films*, vol. 261, pp. 266–270, 1995.
[69] A. C. Dürr, F. Schreiber, M. Kelsch, H. D. Carstanjen, H. Dosch, and O. H. Seeck, "Morphology and interdiffusion behavior of evaporated metal films on crystalline diindenoperylene thin films," *J. Appl. Phys.*, vol. 93, pp. 5201–5209, 2003.
[70] W. J. H. van Gennip, J. K. J. van Duren, P. C. Thüne, R. A. J. Janssen, and J. W. Niemantsverdriet, "The interfaces of poly(*p*-phenylene vinylene) and fullerene derivatives with Al, LiF, and Al/LiF studied by secondary ion mass spectroscopy and x-ray photoelectron spectroscopy: Formation of AlF_3 disproved," *J. Chem. Phys.*, vol. 117, pp. 5031–5035, 2002.
[71] A. J. Maxwell, P. A. Brühwiler, D. Arvanitis, J. Hasselström, M. K.-J. Johansson, and N. Martensson, "Electronic and geometric structure of C_{60} on Al(111) and Al(110)," *Phys. Rev. B*, vol. 57, pp. 7312–7326, 1998.
[72] W. Ma, C. Yang, X. Gong, K. Lee, and A. Heeger, "Thermally stable, efficient polymer solar cells with nanoscale control of the interpenetrating network morphology," *Adv. Funct. Mater.*, vol. 15, pp. 1617–1622, 2005.
[73] V. P. Singh, R. S. Singh, B. Parthasarathy, A. Aguilera, J. Anthony, and M. Payne, "Cooper-phthalocyanine-based organic solar cells with high open-circuit voltage," *Appl. Phys. Lett.*, vol. 86, pp. 082106-1–082106-3, 2005.
[74] J. Wiesecke and M. Rehahn, "Direct observation of alpha-chloro-p-quinodimethane as the real monomer in the Gilch polymerization leading to poly(p-phenylene-vinylene)s," *Macromol. Rapid Commun.*, vol. 28, pp. 188–193, 2007.
[75] E. Schäffer, T. Thurn-Albrecht, T. P. Russel, and U. Steiner, "Electrically induced structure formation and pattern transfer," *Nature*, vol. 403, pp. 874–877, 2000.

Fernando Araujo de Castro graduated (B.Sc.) in physics in 2001, received the M.Sc. degree in 2004 and the Ph.D. degree in organic photovoltaics in 2007 from the University of São Paulo, São Paulo, Brazil.

He was a Postdoctoral Research Fellow in the Laboratory for Functional Polymers, Swiss Federal Laboratories for Materials Testing and Research (EMPA), Duebendorf, Switzerland until the end of 2009. Since 2010, he has been a Senior Research Scientist at the National Physical Laboratory, Materials Division, Teddington, U.K.

Jakob Heier received the Diploma degree in physics from the University of Konstanz, Konstanz, in 1994, and the Ph.D. degree in materials science and engineering from Cornell University, Ithaca, NY, in 1999.

He was engaged in different positions in industry and academia, such as Papyron BV, BiOMaDe Technology Foundation, and Philips DAP. He is currently a Research Scientist in the Laboratory for Functional Polymers, Swiss Federal Laboratories for Materials Testing and Research (EMPA), Duebendorf, Switzerland.

Frank Nüesch graduated in physics from the Eidgenössische Technische Hochschule Zürich (ETHZ), Zurich, Switzerland, in 1989. He received the Ph.D. degree on molecular aggregates and their role in photo-induced charge injection into oxide semiconductors from the École Polytechnique Fédérale de Lausanne, Lausanne, Switzerland, 1995.

During his postdoctoral studies, his research was focused on interfacial dipole layers and their role for charge injection in organic optoelectronic devices. Since April 2004, he has been the Head of the Laboratory for Functional Polymers, Swiss Federal Laboratories for Materials Testing and Research (EMPA), Duebendorf, Switzerland, where he has been engaged in the research on organic solar cells, laser ablation transfer, and dielectric elastomer actuators.

Roland Hany received the Diploma and Ph.D. degrees in physical chemistry from the University of Zürich, Zürich, Switzerland, in 1987 and 1992, respectively.

He is currently a Group Leader in the Laboratory for Functional Polymers, Swiss Federal Laboratories for Materials Testing and Research (EMPA), Duebendorf, Switzerland. His research interests include the properties of biologically produced polyesters and the application of solution-processable semiconducting materials for organic photovoltaics.